A&A 493, 119–125 (2009)
DOI: 10.1051/0004-6361:200810159

Astronomy & Astrophysics

Mid-infrared VISIR and *Spitzer* observations of the surroundings of the magnetar SGR 1806-20⋆

F. Rahoui[1,2], S. Chaty[1], and P.-O. Lagage[1]

[1] Laboratoire AIM, CEA/DSM – CNRS – Université Paris Diderot, IRFU/Service d'Astrophysique, Bât. 709, CEA-Saclay, 91191 Gif-sur-Yvette Cedex, France
e-mail: [frahoui;chaty;pierrre-olivier.lagage]@cea.fr
[2] European Southern Observatory, Alonso de Córdova 3107, Vitacura, Santiago de Chile

Received 8 May 2008 / Accepted 23 October 2008

ABSTRACT

Context. SGR 1806-20 is the soft gamma-ray repeater that has exhibited the highest activity since its discovery, including a giant flare in 2004 December 27. Previous studies of this source – probably a magnetar – have shown that it was associated with a massive star cluster embedded in a gas and dust cloud. Moreover, several stars in the cluster are peculiar hypergiants – luminous blue variable (LBV) and Wolf-Rayet stars – exhibiting strong and likely dusty stellar winds.
Aims. We aimed at studying the mid-infrared emission of the stars associated with the same cluster as SGR 1806-20, to detect variations that could be due to the high-energy activity of the magnetar through interaction with the dust. We also studied the morphology of the cloud close to the centre of the cluster.
Methods. We carried out mid-infrared observations of SGR 1806-20 and its environment, with the highest spatial resolution in this domain to date, using ESO/VISIR in 2005 and 2006, and we retrieved *Spitzer*/IRAC-MIPS archival data of the same field. We performed broadband photometry of three stars – LBV 1806-20, a WC9 and an O/B supergiant – on our VISIR images, as well as on the IRAC data. We then built and fitted their broadband spectral energy distributions with a combination of two absorbed black bodies, representing their stellar components, as well as a possible mid-infrared excess, to derive their physical parameters.
Results. We show that LBV 1806-20 and the WC9 star exhibit a mid-infrared excess, likely because of the presence of circumstellar dust related to their winds. We also show that only LBV 1806-20 has had a variable flux over a period of two years, variability that is due to its LBV nature rather than to a heating of the gas and dust cloud by the high-energy emission of SGR 1806-20. Finally, differences in the intrinsic absorptions of the three stars show an inhomogeneous structure of the density of the gas and dust cloud in the massive star cluster.

Key words. stars: neutron – infrared: stars – dust, extinction – open clusters and associations: general – stars: early-type – supergiants

1. Introduction

Soft gamma-ray repeaters (SGRs) represent a small group – four known objects, three in the Galactic centre and one in the Large Magellanic Cloud – of highly-magnetized exotic pulsars presenting no evidence of binarity. They are characterised by a spin period clustered in the range 6–12 s, and a persistent soft X-ray emission around 10^{35}–10^{36} erg s^{-1}. Their spectra are well-fitted by a combination of a black body ($kT \sim 0.5$–0.6 keV) and a power-law tail ($\Gamma \sim 2.5$), and they also exhibit short and intense bursts (duration of a few hundred milliseconds) of soft γ-rays and hard X-rays. Giant flares have also been observed for three of them: SGR 0526-66, SGR 1806-20, and SGR 1900+14. Recently, persistent hard X-ray emission has been detected on SGR 1806-20 (Mereghetti et al. 2005).

As for anomalous X-ray pulsars (AXPs), proposed to be strongly related to SGRs due to their similar characteristics (Gavriil et al. 2002), the likely source of their radiative emission is not accretion like for other neutron stars but their very strong magnetic field (10^{14}–10^{15} G) (see e.g. Mereghetti et al. 2002; Woods & Thompson 2006, for recent reviews). It is now commonly accepted that SGRs and AXPs are magnetars, i.e. neutron stars whose high-energy emission (persistent and transient) is powered by the decay of a very strong dipole-like magnetic field (Duncan & Thompson 1992; Thompson & Duncan 1995, 1996).

SGR 1806-20 is the SGR that has exhibited the highest activity since its discovery (Atteia et al. 1987; Laros et al. 1987). It is located towards the Galactic centre, and it exhibits 7.47 s pulsations (Kouveliotou et al. 1998) and an 8.3×10^{-11} s s^{-1} spin-down rate. It entered an active phase in 2003 and exhibited bursts up to late 2004. Finally, a giant flare (corresponding to 10^{47}–10^{48} erg s^{-1} for a distance between 8 and 15 kpc) occurred in 2004 December 27 (Hurley et al. 2005), and a remnant radio afterglow allowed an accurate localisation of the source (Gaensler et al. 2005).

LBV 1806-20, a luminous blue variable (LBV), was long believed to be its near-infrared (NIR) counterpart (Kulkarni et al. 1995), but Kaplan et al. (2002) showed that the SGR was 12″ away from the LBV using *Chandra* observations. The accurate localisation of the source, as well as an exhaustive monitoring finally led to the detection of the NIR counterpart of SGR 1806-20 (Israel et al. 2005; Kosugi et al. 2005) by observing a variability correlated to the high-energy emission, as for AXPs, which strengthens the connection between both objects.

The environment of SGR 1806-20 is very young and dusty, and it is then relevant to observe it at mid-infrared (MIR) wavelengths and search for variabilities correlated to the high-energy emission. Indeed, Fuchs et al. (1999) and Eikenberry et al. (2001) show that it was associated with a massive star cluster,

⋆ Based on observations carried out at the European Southern Observatory under programmes ID 075.D-0773 and 077.D-0721 (P.I. Chaty).

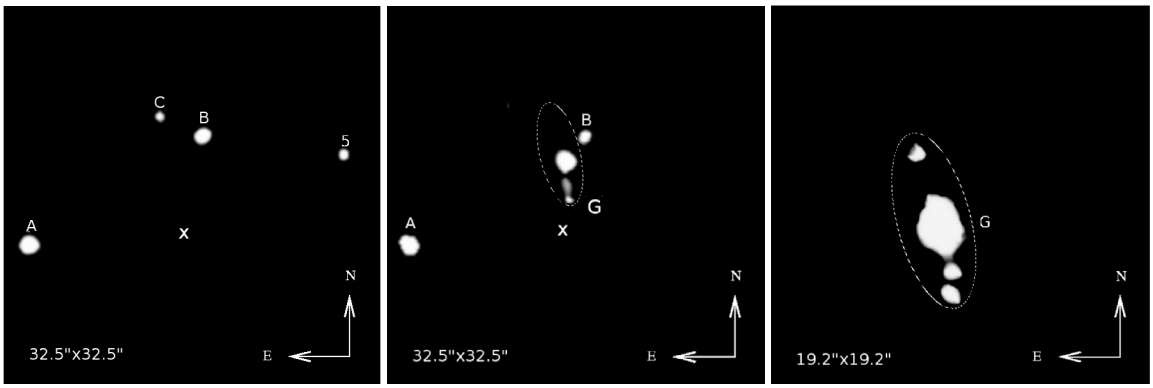

Fig. 1. PAH1 (*left*, 0.″127 plate scale per pixel), PAH2 (*centre*, 0.″127 plate scale per pixel), and Q2 (*right*, 0.″075 plate scale per pixel) VISIR images of the environment of SGR 1806-20 (white X point) obtained in June 2006. A is LBV 1806-20, B is a WC9 star, C is an O/B supergiant, and 5 is a red giant (Eikenberry et al. 2004; Figer et al. 2005). An ellipse pattern surrounds G, the hottest part of the gas and dust cloud in which all stars are embedded. We detected it in PAH2 and in Q2.

along with LBV 1806-20. Moreover, this cluster is located inside the radio nebula G10.0-0.3, powered by the very strong winds of the LBV (Gaensler et al. 2001). Finally, this radio nebula itself is associated with the giant molecular complex W31 (Corbel et al. 1997). Corbel & Eikenberry (2004) showed that W31 was resolved into two components, one at $d \sim 4$ kpc with $A_v \sim 15$ and another one at $d \sim 15.1$ kpc with $A_v = 37 \pm 3$, and that LBV 1806-20 (and consequently the massive star cluster, and SGR 1806-20) belonged to the further component of W3, suggesting a distance of $15.1^{+1.8}_{-1.3}$ kpc. Nevertheless, Bibby et al. (2008) recently performed high-resolution near-infrared spectroscopy of O/B and Wolf-Rayet stars in the cluster to derive their accurate spectral classification. This allowed them to use both synthetic photometry and isochrone fitting to derive a distance modulus of 14.7 ± 0.35 mag for the cluster, which corresponds to a distance of $8.7^{+1.8}_{-1.5}$ kpc.

In this paper, we report MIR observations - with the highest spatial resolution in this domain to date – of SGR 1806-20 and its environment, carried out at ESO/VLT with VISIR in June 2005 and 2006. We also report archival data obtained at three different epochs between 2004 and 2006 with IRAC and MIPS mounted on *Spitzer*. Our goal was to detect any MIR variability that could be due to the high-energy activity of the SGR, as well as to study the morphology of the gas and dust cloud in which all sources are embedded.

In Sect. 2, we describe these observations and their analysis. In Sect. 3, we present the broadband spectral energy distributions (SEDs) we built for three sources using the VISIR and IRAC fluxes obtained in 2005 and 2006. For each year, there were no more than three months between the VISIR and the IRAC observations, which allowed us to fit these SEDs to derive the physical parameters of the stars with contemporaneous data from 3.6 μm to 11.25 μm. In Sect. 4, we analyse the results and discuss the MIR variability, the intrinsic absorption, and the distance of these stars, as well as the MIR emission of SGR 1806-20.

2. Observations and data reduction

2.1. ESO/VISIR data

The MIR observations were carried out on 2005 June 20−22 and 2006 June 29−30 using VISIR (Lagage et al. 2004), the ESO/VLT mid-infrared imager and spectrograph, composed of an imager and a long-slit spectrometer covering several filters in N and Q bands and mounted on Unit 3 of the VLT (Melipal). The standard "chopping and nodding" MIR observational technique was used to suppress the background dominating at these wavelengths. Secondary mirror-chopping was performed in the north-south direction with an amplitude of 16″ at a frequency of 0.25 Hz. Nodding technique, needed to compensate for chopping residuals, was chosen as parallel to the chopping and applied using telescope offsets of 16″. Because of the high thermal MIR background for ground-based observations, the detector integration time was set to 16 ms.

We performed broadband photometry in three filters, PAH1 ($\lambda = 8.59 \pm 0.42$ μm), PAH2 ($\lambda = 11.25 \pm 0.59$ μm), and Q2 ($\lambda = 18.72 \pm 0.88$ μm), using the large field in all bands (32.″5 × 32.″5 and 0.″127 plate scale per pixel) in June 2005. In June 2006, we used the large field in PAH1 and PAH2 and the small one (19.″2 × 19.″2 and 0.″075 plate scale per pixel) in Q2. All the observations were bracketed with standard star observations for flux calibration and PSF determination. The weather conditions were good and stable during the observations.

Raw data were reduced using the IDL reduction package written by Pantin. The elementary images were co-added in real time to obtain chopping-corrected data, then the different nodding positions were combined to form the final image. The VISIR detector is affected by stripes randomly triggered by some abnormal high-gain pixels. A dedicated destriping method was developed (Pantin 2008, in prep.) to suppress them.

The filtered reduced images of 2006 are displayed in Fig. 1. These images were cleaned using the multiresolution software package written by Starck[1] and presented in Starck & Murtagh (1998), which performs background and noise modelling, as well as noise subtraction using multiresolution tools. Nevertheless, we performed photometry on the unfiltered images using aperture photometry, and the fluxes in all bands are listed in Table 1. We kept the same labels as Eikenberry et al. (2004, EML04 hereafter) and Figer et al. (2005) for all the detected stars. A is therefore LBV 1806-20, B is a WC9 star, C is an O/B supergiant, and 5 is a red giant. Finally, G is a hot and dense part of the gas and dust cloud, which is the likely birth site of the massive star cluster and is only visible in the MIR domain. On June 2005, the exposure time was 600 s in all bands, while it was 1200 s in PAH1 and PAH2 and 2400 s in Q2 in June 2006, which explains why we detected neither C in PAH1 nor G in PAH2 in June 2005, their fluxes being too low

[1] http://thames.cs.rhul.ac.uk/~multires/mr4-software/index.html

Table 1. Summary of VISIR observations of the sources in the environment of SGR 1806-20. We give their name and their MIR fluxes (in Jy) in the PAH1 (8.59 μm), PAH2 (11.25 μm), and Q2 (18.72 μm) filters. When we did not detect the source, we give its upper limit. For the dust cloud, we give the upper limit for an extended source covering 450 pixels in PAH1 and PAH2, as this corresponds to the area covered by the dust cloud when we detected it in PAH2 in June 2006. Uncertainties are given at 1σ.

Sources	PAH1	PAH2	Q2
		June 2005	
LBV 1806-20 (A)	0.133 ± 0.004	0.089 ± 0.005	<0.058
WC9 (B)	0.077 ± 0.003	0.057 ± 0.004	<0.058
Supergiant (C)	<0.0126	<0.0149	<0.058
Red Giant (5)	0.020 ± 0.002	<0.0149	<0.058
Dust (G)	<0.091	<0.111	2.60 ± 0.20
		June 2006	
LBV 1806-20 (A)	0.103 ± 0.004	0.067 ± 0.004	<0.051
WC9 (B)	0.076 ± 0.003	0.053 ± 0.003	<0.051
Supergiant (C)	0.012 ± 0.002	<0.0124	<0.051
Red Giant (5)	0.019 ± 0.002	<0.0124	<0.051
Dust (G)	<0.112	0.078 ± 0.007	2.82 ± 0.14

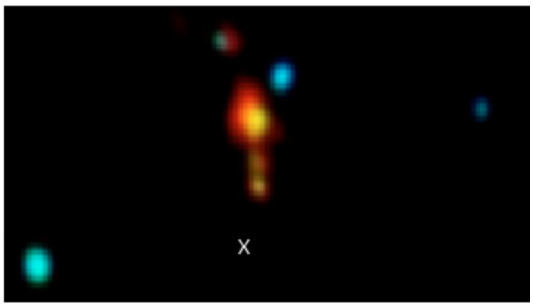

Fig. 2. Three-colour image of the environment of SGR 1806-20 (white X point) done with images of June 2006; PAH1 is in blue, PAH2 in green, and Q2 in red. Q2 image was rescaled to a 0.″127 plate scale. The cloud detected with VISIR appears to be splitted into several components, which shows that its temperature is not homogeneous, the cloud being hotter in the centre of the massive star cluster.

compared to the sensitivity we were able to reach (see Table 1). A three-colour image (made with PAH1, PAH2, and Q2 images) is also displayed in Fig. 2 and we clearly see that the gas and dust cloud emits mostly beyond 11 μm.

2.2. Spitzer/IRAC-MIPS archival data

We searched for MIR public data of the star cluster in the archives of the *Spitzer Space Telescope*. We found photometric data taken at three different epochs, 2004 October 29, 2005 September 27, and 2006 April 10, in the *Spitzer*'s Galactic Legacy Infrared Mid-Plane Survey Extraordinaire (GLIMPSE, Benjamin et al. 2003), survey of the Galactic plane ($|b| \leq 1°$ and between $l = 10°$ and $l = 65°$ on both sides of the Galactic centre), using the IRAC camera in four bands, 3.6 ± 0.745 μm, 4.5 ± 1.023 μm, 5.8 ± 1.450 μm, and 8.0 ± 2.857 μm. The IRAC plate scale is 1.″2 per pixel and the field of view is 5.′2 × 5.′2. We also found archival MIPS data of the same field at 24 μm.

We performed photometry of the stars A, B, and C we had detected with VISIR on the post-basic calibration data (post-BCD) using the software *StarFinder*, part of the *Scisoft* package from ESO, well-suited for point-source photometry in crowded fields. Post-BCD data are raw data on which the *Spitzer* pipeline performs dark subtraction, multiplexer bleed correction, detector linearization, flat-fielding, cosmic ray detection, flux calibration, pointing refinement, mosaicking, and coaddition. The images taken in September 2005 are displayed in Fig. 3, and fluxes for each epoch are listed in Table 2. Moreover, Fig. 4 displays the MIPS image of the same field at 24 μm.

3. Absorption and SEDs

3.1. Absorption

The absorption at wavelength λ, A_λ, is a crucial parameter to fit the SEDs, especially in the MIR. Indeed, inaccurate values can lead to a false assessment of the dust emission. The visible absorption A_v was a free parameter of the fits. An accurate interstellar absorption law – i.e. the wavelength dependence of the $\frac{A_\lambda}{A_v}$ ratio in the line of sight – was then needed to properly fit the SEDs.

From 1.25 μm to 8.0 μm, we used the analytical expression given in Indebetouw et al. (2005). They derived it from the measurements of the mean values of the colour excess ratios $\frac{A_\lambda - A_J}{A_J - A_K}$ from the colour distributions of observed stars in the direction of the Galactic centre. They used archival data from the GLIMPSE catalogue, which is relevant in our case. Beyond 8.0 μm, where absorption is dominated by the silicate features at 9.7 μm and 18.0 μm, we used the extinction law from Lutz et al. (1996), which includes the interstellar silicate absorption at 9.7 μm. The $\frac{A_\lambda}{A_v}$ values we used in each band are listed in Table 3.

3.2. SEDs

With all the observational and archival data from NIR to MIR wavelengths, we built the 2005 and 2006 SEDs of these sources. We fitted them (χ^2 minimisation) using a combination of two absorbed black bodies, one representing the companion star emission and one representing a MIR excess, if there was any:

$$\lambda F(\lambda) = \frac{2\pi hc^2}{{D_*}^2 \lambda^4} 10^{-0.4 A_\lambda} \left[\frac{{R_*}^2}{e^{\frac{hc}{\lambda k T_*}} - 1} + \frac{{R_\mathrm{D}}^2}{e^{\frac{hc}{\lambda k T_\mathrm{D}}} - 1} \right] \text{in W m}^{-2}. \quad (1)$$

We added to the data uncertainties systematic errors as follows:

– a 2% systematic error in each IRAC band as given in the IRAC manual[2];

[2] http://ssc.spitzer.caltech.edu/documents/som/som8.0.irac.pdf

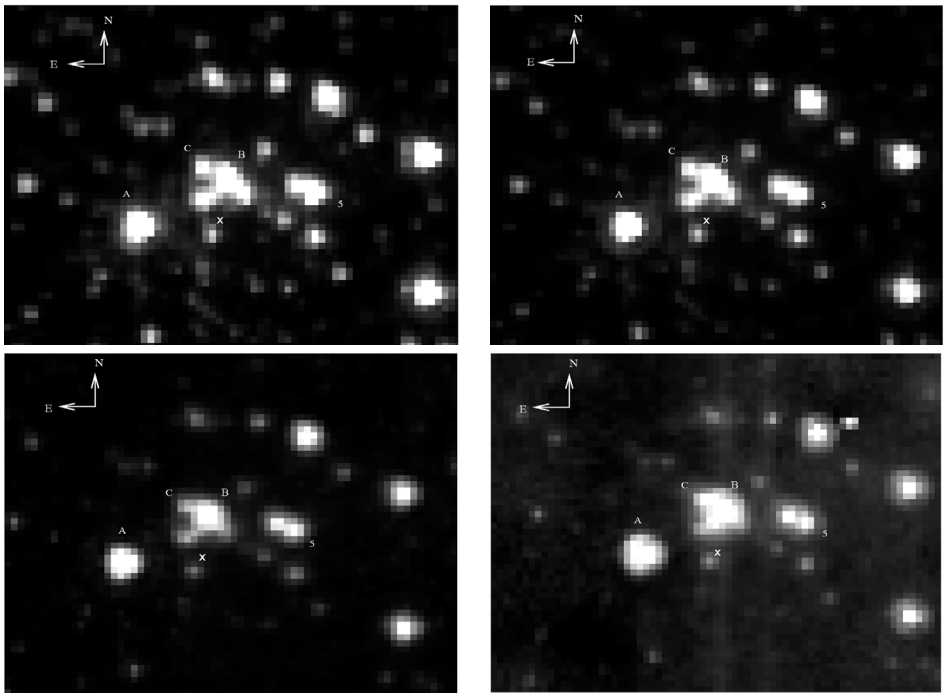

Fig. 3. IRAC 3.6 μm (*top left*), 4.5 μm (*top right*), 5.8 μm (*bottom left*), and 8.0 μm (*bottom right*) images of the environment of SGR 1806-20 (white X point). The field of view is about $79'' \times 71''$ and the plate scale is $1''.2$ per pixel. We point out that the position of SGR 1806-20 is $2''.95$ away from the point source located south east of the white X point, which – considering the $0''.5$ astrometric accuracy of the *Spitzer* telescope – excludes an association with SGR 1806-20.

Table 2. Summary of IRAC observations of the sources in the environment of SGR 1806-20. We give their name and their MIR fluxes (in Jy). Uncertainties are given at 1σ.

Sources	3.6 μm	4.5 μm	5.8 μm	8.0 μm
		October 2004		
LBV 1806-20 (A)	0.306 ± 0.010	0.316 ± 0.008	0.283 ± 0.008	0.175 ± 0.005
WC9 (B)	0.165 ± 0.005	0.208 ± 0.006	0.218 ± 0.007	0.141 ± 0.003
Supergiant (C)	0.041 ± 0.002	0.036 ± 0.002	0.028 ± 0.002	0.027 ± 0.002
		September 2005		
LBV 1806-20 (A)	0.337 ± 0.015	0.332 ± 0.016	0.299 ± 0.014	0.199 ± 0.007
WC9 (B)	0.172 ± 0.009	0.218 ± 0.011	0.224 ± 0.011	0.140 ± 0.005
Supergiant (C)	0.037 ± 0.003	0.037 ± 0.003	0.031 ± 0.003	0.027 ± 0.001
		April 2006		
LBV 1806-20 (A)	0.297 ± 0.010	0.304 ± 0.001	0.272 ± 0.011	0.174 ± 0.005
WC9 (B)	0.170 ± 0.006	0.207 ± 0.007	0.225 ± 0.009	0.140 ± 0.006
Supergiant (C)	0.041 ± 0.003	0.038 ± 0.002	0.030 ± 0.003	0.025 ± 0.002

– comparing the variations in the flux calibration values obtained from the standard stars with VISIR during our observation nights, we figured out that systematic errors were about 5% at 10 μm and 10% at 20 μm.

The free parameters of the fits were the absorption in the V band A_v, the companion star black body temperature T_*, and its radius-to-distance ratio $\frac{R_*}{D_*}$, as well as the MIR excess spherical component black body temperature and radius $T_{\rm D}$ and $R_{\rm D}$. The best-fitting parameters for individual sources, as well as the corresponding χ^2, are listed in Table 4, and fitted SEDs of objects A–C are displayed in Fig. 5.

4. Results and discussion

4.1. The variability of LBV 1806-20

The fluxes listed in Tables 1 and 2 show that LBV 1806-20 is variable in the MIR, in all bands from 3.6 μm to 11.25 μm. Indeed, the IRAC fluxes substantially increased from October 2004 to September 2005, and then decreased from September 2005 to April 2006 to reach a similar level to the one in October 2004. Concerning the VISIR fluxes, we unfortunately do not have any data taken in 2004. Nevertheless, the same decrease in the MIR flux is observed from June 2005 to June 2006 in both PAH1 and PAH2.

In a previous spectroscopic and photometric study of LBV 1806-20, EML04 confirmed the likely LBV nature of this star (van Kerkwijk et al. 1995) with spectral classes 09-B2, and showed that there were strong anticorrelated variations in the equivalent widths of He I 2.112 μm and Br γ lines, which led to correlated variations of the star temperature and the number of ionising photons. Moreover, comparison with previous photometry (Kulkarni et al. 1995) have shown that the variation in temperature did not result in the variation in the K band magnitude of the star. As a possible explanation, they proposed either an anticorrelated variation in the star temperature and radius,

Table 3. Adopted $\frac{A_\lambda}{A_v}$ values.

Filters	J	H	Ks	3.6 μm	4.5 μm	5.8 μm	8.0 μm	8.59 μm	11.25 μm
$\frac{A_\lambda}{A_v}$	0.289	0.174	0.115	0.064	0.054	0.047	0.044	0.060	0.061

Table 4. Summary of parameters we used to fit the SEDs of the sources. We give their name and then the parameters themselves: the extinction in the optical A_v, the temperature T_* and the $\frac{R_*}{D_*}$ ratio of the star, and the temperature T_D and radius R_D (in R_* unit) of the dust component. We also add the reduced χ^2 we reach for each fit, as well as the uncertainties on the parameters.

Sources	A_v	$T_*[\Delta T_*]$(K)	$\frac{R_*}{D_*}$	T_D(K)	R_D (R_*)	χ^2/d.o.f.
LBV 1806-20 (A) (2005)	$28.6^{+1.5}_{-1.5}$	21 500 [17 900–26 200]	$3.08^{+0.36}_{-0.48} \times 10^{-10}$	1130^{+130}_{-110}	$8.4^{+1.0}_{-0.9}$	3.1/4
LBV 1806-20 (A) (2006)	$29.0^{+1.2}_{-1.2}$	17 600 [15 000–21 200]	$3.68^{+0.24}_{-0.36} \times 10^{-10}$	1020^{+140}_{-100}	$6.5^{+0.7}_{-0.7}$	3.9/4
WC9 (B)	$35.2^{+1.4}_{-1.8}$	53 000 [25 000–71 000]	$4.36^{+1.36}_{-0.68} \times 10^{-11}$	1850^{+60}_{-120}	$46.0^{+8.0}_{-14.0}$	6.8/4
Supergiant (C)	$31.8^{+0.8}_{-2.1}$	25 700 [11 600–40 500]	$1.38^{+0.62}_{-0.36} \times 10^{-10}$			6.0/5

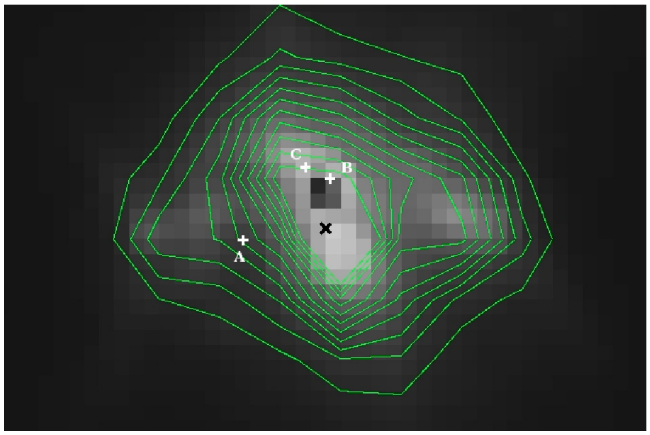

Fig. 4. MIPS 24 μm image of the environment of SGR 1806-20 (black X point). We also superimposed the MIPS contour plot to stress the differences in luminosity. We clearly see the gas and dust cloud in which all the stars are embedded, and it is likely the birth site of the massive star cluster. It appears that LBV 1806-20 (A) is located in a less dense and colder zone of the cloud than the WC9 star (B) and the O/B supergiant star (C), which explains that its intrinsic absorption is lower. Moreover, the central part of the cloud – which appears saturated in this image as it is too hot with respect to the MIPS level of saturation – corresponds to the region detected with VISIR. The field of view is 94″ × 67″ and the plate scale is 2.″5 per pixel.

which is typical of some LBV stars (Humphreys & Davidson 1994; Morris et al. 1996), or an increase in the stellar wind density, resulting in more absorbed ultraviolet continuum photons, consequently, more emission lines.

To investigate the origin of the MIR flux variation of LBV 1806-20, and to find out whether it was related to one of the previously described mechanisms or to the heating of the gas and dust cloud by the high-energy emission of SGR 1806-20, we built its broadband SED using 2005 and 2006 IRAC and VISIR data – as well as the NIR magnitudes from EML04, the NIR flux being marginally variable – and fitted it. The best-fitting parameters are listed in Table 4.

The presence of warm circumstellar dust around LBV stars is common (see e.g. McGregor et al. 1988, about AG Car), as they are often associated with ejected dusty nebulae, and a component of warm dust is necessary to explain the huge MIR excess LBV 1806-20 exhibits.

Moreover, the fits suggest a change from a B1 (T_* = 21 500 K) to a B3 (T_* = 17 600 K) spectral type, and at least a 20% increase in the stellar radius ($R_* = 3.08 \times 10^{-10} \times D_*$ to $R_* = 3.68 \times 10^{-10} \times D_*$) from 2005 to 2006. Meanwhile, the dust temperature decreased by about 10% (T_D = 1130 K to T_D = 1020 K), while the dust radius (decrease of about 7.5% from $R_D = 25.87 \times 10^{-10} \times D_*$ to $R_D = 23.92 \times 10^{-10} \times D_*$) was roughly constant, considering the uncertainties on the star radius and distance (about 17%).

Under the assumption that a dust grain is a perfect black body – i.e. it fully absorbs the received flux – and that the star emission is not absorbed before reaching the dust, the equation of thermodynamical equilibrium between a dust grain and the star can be written as

$$\sigma T_*^4 \left(\frac{R_*}{R_D}\right)^2 = 4 \times \int_0^\infty Q(\nu) B(T_D, \nu) \mathrm{d}\nu \qquad (2)$$

where $B(T_D, \nu)$ is the dust grain black body emission at the frequency ν, and $Q(\nu)$ the dust grain emissivity, approximated as $Q(\nu) = Q_0 \nu^n$, where Q_0 is a constant and $1 \leq n \leq 2$ (Draine & Lee 1984).

The expected grain temperature can therefore be written as

$$T_D = \left[\left(\frac{\pi^4}{60 Q_0}\right)\left(\frac{h}{k}\right)^n \frac{1}{\Gamma(4+n)\zeta(4+n)} \left(\frac{R_*}{R_D}\right)^2 T_*^4\right]^{\frac{1}{4+n}} \qquad (3)$$

where h and k are the Planck and the Boltzmann constants, respectively, Γ the gamma function, and ζ the Riemann zeta function.

By studying the properties of the warm dust around the LBV HD 168625, Robberto & Herbst (1998) give $Q_0 = 1.52 \times 10^{-8} \times a$ – where a is the dust grain radius – and find $a \sim 1$ μm, consistent with LBVs having large dust grains ($a \geq 0.1$ μm) in their winds, as shown in Mitchell & Robinson (1986) for η Car and McGregor et al. (1988) and Shore et al. (1996) for AG Car.

With Q_0 given in Robberto & Herbst (1998), a large dust grain size $a \sim 0.5$ μm, and $n = 1.2$ as given in Rouleau & Martin (1991), we find $T_D \sim 1143$ K in 2005, and $T_D \sim 1081$ K in 2006, i.e. a decrease of about 6%, in good agreement with what we obtain in our best fits. This is therefore consistent with an MIR flux variation of LBV 1806-20 due to the anticorrelated variations in the star temperature and radius rather than to a heating or a cooling of the gas and dust cloud due to the high-energy activity of SGR 1806-20.

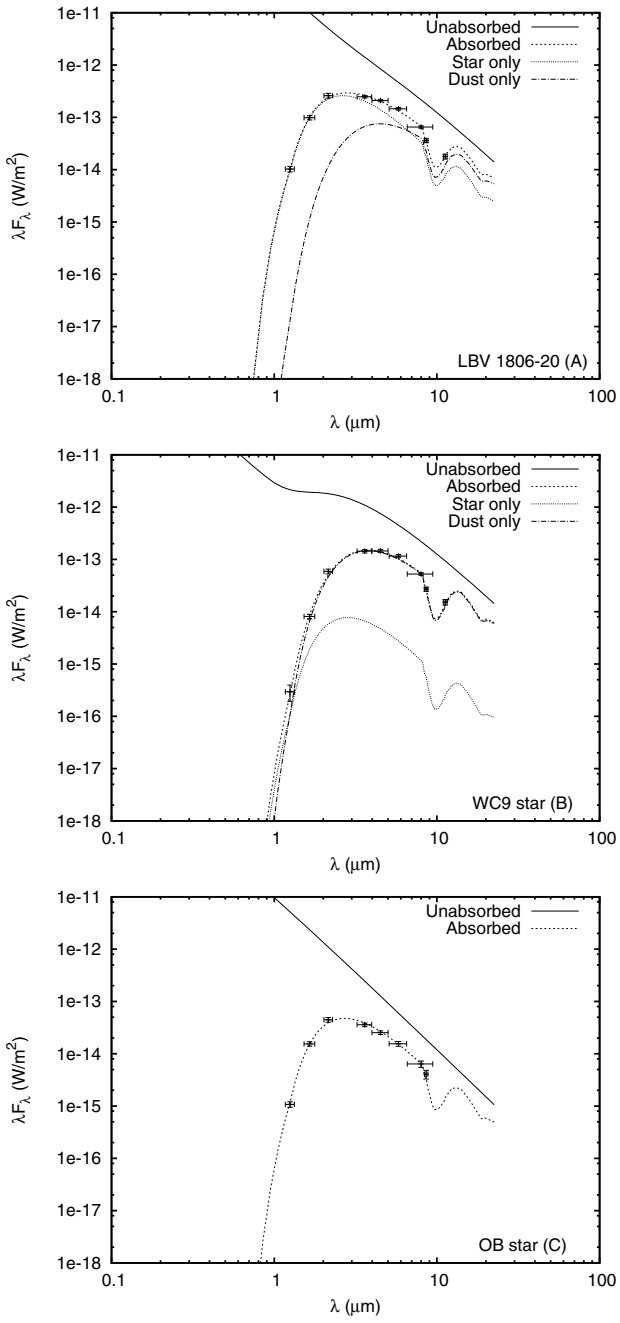

Fig. 5. NIR to MIR−fitted SEDs of LBV 1806-20, the WC9 star, and the O/B supergiant. For LBV 1806-20 and the WC9 star, we also add parts of their emission due to the stellar and the dust components. We used the MIR data from the VISIR observations we performed, the GLIMPSE survey, as well as the NIR data from EML04. The silicate absorption feature at 9.7 μm comes from the use of the Lutz's interstellar extinction law, in which it is included.

4.2. Stars B and C

Star B was classified as a WC9 Wolf-Rayet (EML04), and the fluxes listed in Tables 1 and 2 show that its MIR emission was constant in all bands from 3.6 μm to 11.25 μm. We then fitted its SED using the MIR fluxes of 2006 and the NIR magnitudes found in EML04, and the best-fitting parameters are listed in Table 4. Our results suggest that B is extremely reddened and that it exhibits a very large MIR excess. The presence of such excess is typical of WC9 stars, whose C-rich stellar winds allow the creation of circumstellar dust. Moreover, Fig. 5 shows that beyond 1.6 μm (H band), the star barely contributes to the emission, which is also common for WC9 stars (van der Hucht et al. 1996; Crowther et al. 2006). All the fits with a more balanced contribution of the stellar and the dust components (reduced $\chi^2 \geq 3$) or with only a stellar component (reduced $\chi^2 \geq 100$) failed to reproduce the SED. Moreover, we point out that, although $T_{\rm D} = 1850$ K is high, it is still below the sublimation temperature of amorphous carbon found around WC9 stars (~2000 K, see for instance Laor & Draine 1993; Preibisch et al. 1993).

Star C was found to be either an O/B supergiant or a hypergiant through spectroscopy (EML04), but Figer et al. (2005) then performed higher resolution spectroscopy and derived an O/BI spectral class, with narrower lines than previously found. Their result is confirmed by Bibby et al. (2008), who derive a B1−B3I spectral type through high-resolution NIR spectroscopy. We unfortunately did not detect C during our first VISIR run in June 2005 as our exposure time was not sufficient, preventing us from performing a comparison with the flux of 2006 June. Nevertheless, the IRAC fluxes listed in Table 2 point out towards a constant MIR flux from 2004 to 2006 in all bands. Using the NIR magnitudes given in EML04, as well as the IRAC and the VISIR fluxes of 2006, we fitted its SED and the best-fitting parameters are listed in Table 4.

The best-fitting temperature is typical of an early-B supergiant star. Moreover, if we assume that the star C is associated with the cluster, it is then possible to get its radius by multiplying the best-fitting radius-to-distance ratio derived from our fit by the distance of the cluster. If we use the distance of $15.1^{+1.8}_{-1.3}$ kpc given in Corbel & Eikenberry (2004), we derive a radius $R_* = 92.4^{+53.2}_{-32.1}\ R_\odot$, while we find $R_* = 53.2^{+30.6}_{-18.5}\ R_\odot$ for a distance of $8.7^{+1.8}_{-1.5}$ kpc (Bibby et al. 2008). The latter is more consistent with the expected radius of a normal B1−B3 supergiant star, therefore favouring the distance given in Bibby et al. (2008).

Finally, we would like to point out that the three-colour image displayed in Fig. 2 interestingly suggests that C is associated with the northern part of the gas and dust cloud, since the cloud emission reappears at the supergiant position. If this were confirmed, it would mean that the cloud is heated by C.

4.3. SGR 1806-20

High-energy emission of magnetars is believed to be powered by the magnetic energy of their very strong magnetic field. Moreover, five AXPs and SGR 1806-20 have been detected in the optical bands and/or the NIR, and all of them were found to exhibit a variable NIR emission correlated to the X-ray emission. This optical/NIR emission is explained either as the non-thermal radiation by particles in the magnetosphere or as the irradiation by the X-ray emission of a fossile passive dust disk around the neutron star.

The second explanation recently received some credit as the AXP 4U 0142+61 has been detected in the MIR using IRAC at 4.5 μm and 8 μm (Wang et al. 2006). It is shown that its IR emission can be understood by the presence of an X-ray heated disk. This disk would have formed from the fallback material of a supernova, and would emit mostly in the IR consequently to the irradiation by the high-energy emission of the neutron star. Moreover, the authors derive an unabsorbed MIR to X-ray flux ratio $\nu_{4.5\ \mu{\rm m}} F_{4.5\ \mu{\rm m}} / F_{\rm X} \sim 3.4 \times 10^{-4}$, where $F_{\rm X}$ is the unabsorbed 2−10 keV X-ray flux.

SGR 1806-20 has never been detected in the MIR domain, neither with IRAC nor with VISIR, as shown in the images displayed in this paper. Indeed, considering that the MIR emission of SGR 1806-20 would be due to an irradiated fallback disk and that the unabsorbed MIR to X-ray flux ratio derived in Wang et al. (2006) is typical of dust disks around young neutron stars, we can expect the SGR 1806-20 absorbed flux at 4.5 μm to be below 10 μJy, one order of magnitude below the sensitivity of about 200 μJy at 5σ of the GLIMPSE survey.

4.4. Absorption

All the intrinsic absorptions derived from our fits show that stars B and C are likely more absorbed than LBV 1806-20, as they are embedded in a hotter and denser part of the associated cloud of dust and gas visible on our VISIR images in PAH2 and Q2 (see Fig. 2). Indeed, Fig. 4 displays an MIPS image of the environment of SGR 1806-20 at 24 μm with contour plots. Because the *Spitzer* sensitivity is far better, a larger part of the cloud is visible. We see that LBV 1806-20 (A) is located in a colder and less dense zone than the WC9 star (B) and the B supergiant star (C), which both are closer to the core of the cloud. The image is saturated, and the saturated pixels correspond to the zone of the cloud detected with VISIR (taking into account the difference of plate scale per pixel in both images, 0.″075 for VISIR and 2.″5 for MIPS). Star B is then likely very close to the hottest and densest zone of the dust cloud, which is why it exhibits the highest intrinsic absorption. We nevertheless point out that a limitation to this conclusion is that we only see the cloud integrated along the line of sight.

5. Conclusions

We reported the mid-infrared photometry of three stars and the gas and dust cloud associated with the same massive star cluster as SGR 1806-20, using ESO/VISIR and *Spitzer*/IRAC-MIPS data obtained at different epochs between 2004 and 2006.

We show that LBV 1806-20 is the only object to exhibit a likely MIR variability and that this flux variation is probably the consequence of its LBV nature rather than a heating of its circumstellar dust by the giant flare exhibited by SGR 1806-20. We also show that the stars in the central zone of the massive star cluster appear more absorbed, as they are closer to the hottest and densest part of the gas and dust cloud in which all of them are embedded.

Finally, we recommend further high-sensitivity and long-exposure MIR observations of SGR 1806-20 in order to try to detect it, and perhaps constrain the origin of the AXPs and SGRs optical/IR emission.

Acknowledgements. We are pleased to thank the anonymous referee for useful comments, as well as E. Pantin for his IDL code – part of the ESO/VISIR reduction pipeline – we used to reduce our VISIR data, and J. L. Starck for his wavelets package that we used to clean our images. F.R. acknowledges the CNRS/INSU for the funding of the third year of his ESO/CEA studentship. This research has made use of NASA's Astrophysics Data System, of the SIMBAD and VizieR databases operated at CDS, Strasbourg, France, of products from, as well as products from the Galactic Legacy Infrared Mid-Plane Survey Extraordinaire, which is a *Spitzer Space Telescope* Legacy Science Program.

References

Atteia, J.-L., Boer, M., Hurley, K., et al. 1987, ApJ, 320, L105
Benjamin, R. A., Churchwell, E., Babler, B. L., et al. 2003, PASP, 115, 953
Bibby, J. L., Crowther, P. A., Furness, J. P., & Clark, J. S. 2008, MNRAS, 386, L23
Corbel, S., & Eikenberry, S. S. 2004, A&A, 419, 191
Corbel, S., Wallyn, P., Dame, T. M., et al. 1997, ApJ, 478, 624
Crowther, P. A., Morris, P. W., & Smith, J. D. 2006, ApJ, 636, 1033
Draine, B. T., & Lee, H. M. 1984, ApJ, 285, 89
Duncan, R. C., & Thompson, C. 1992, ApJ, 392, L9
Eikenberry, S. S., Garske, M. A., Hu, D., et al. 2001, ApJ, 563, L133
Eikenberry, S. S., Matthews, K., LaVine, J. L., et al. 2004, ApJ, 616, 506
Figer, D. F., Najarro, F., Geballe, T. R., Blum, R. D., & Kudritzki, R. P. 2005, ApJ, 622, L49
Fuchs, Y., Mirabel, F., Chaty, S., et al. 1999, A&A, 350, 891
Gaensler, B. M., Slane, P. O., Gotthelf, E. V., & Vasisht, G. 2001, ApJ, 559, 963
Gaensler, B. M., Kouveliotou, C., Gelfand, J. D., et al. 2005, Nature, 434, 1104
Gavriil, F. P., Kaspi, V. M., & Woods, P. M. 2002, Nature, 419, 142
Humphreys, R. M., & Davidson, K. 1994, PASP, 106, 1025
Hurley, K., Boggs, S. E., Smith, D. M., et al. 2005, Nature, 434, 1098
Indebetouw, R., Mathis, J. S., Babler, B. L., et al. 2005, ApJ, 619, 931
Israel, G., Covino, S., Mignani, R., et al. 2005, A&A, 438, L1
Kaplan, D. L., Fox, D. W., Kulkarni, S. R., et al. 2002, ApJ, 564, 935
Kosugi, G., Ogasawara, R., & Terada, H. 2005, ApJ, 623, L125
Kouveliotou, C., Dieters, S., Strohmayer, T., et al. 1998, Nature, 393, 235
Kulkarni, S. R., Matthews, K., Neugebauer, G., et al. 1995, ApJ, 440, L61
Lagage, P. O., Pel, J. W., Authier, M., et al. 2004, The Messenger, 117, 12
Laor, A., & Draine, B. T. 1993, ApJ, 402, 441
Laros, J. G., Fenimore, E. E., Klebesadel, R. W., et al. 1987, ApJ, 320, L111
Lutz, D., Feuchtgruber, H., Genzel, R., et al. 1996, A&A, 315, L269
McGregor, P. J., Hyland, A. R., & Hillier, D. J. 1988, ApJ, 334, 639
Mereghetti, S., Chiarlone, L., Israel, G. L., & Stella, L. 2002, in Neutron Stars, Pulsars, and Supernova Remnants, ed. W. Becker, H. Lesch, & J. Trümper, 29
Mereghetti, S., Götz, D., Mirabel, I. F., & Hurley, K. 2005, A&A, 433, L9
Mitchell, R. M., & Robinson, G. 1986, MNRAS, 222, 347
Morris, P. W., Eenens, P. R. J., Hanson, M. M., Conti, P. S., & Blum, R. D. 1996, ApJ, 470, 597
Preibisch, T., Ossenkopf, V., Yorke, H. W., & Henning, T. 1993, A&A, 279, 577
Robberto, M., & Herbst, T. M. 1998, ApJ, 498, 400
Rouleau, F., & Martin, P. G. 1991, ApJ, 377, 526
Shore, S. N., Altner, B., & Waxin, I. 1996, AJ, 112, 2744
Starck, J.-L., & Murtagh, F. 1998, PASP, 110, 193
Thompson, C., & Duncan, R. C. 1995, MNRAS, 275, 255
Thompson, C., & Duncan, R. C. 1996, ApJ, 473, 322
van der Hucht, K. A., Morris, P. W., Williams, P. M., et al. 1996, A&A, 315, L193
Wang, Z., Chakrabarty, D., & Kaplan, D. L. 2006, Nature, 440, 772
Woods, P. M., & Thompson, C. 2006, Soft gamma repeaters and anomalous X-ray pulsars: magnetar candidates, Compact stellar X-ray sources, 547